Skyrmion-bimeron dynamic conversion in magnetic nanotracks

M. A. Castro,[1] D. Altbir,[1,2] D. Galvez-Poblete,[1] R. M. Corona,[1] S. Oyarzún,[1] A. R. Pereira,[3] S. Allende,[1,*] and V. L. Carvalho-Santos[3]

[1]*Departamento de Física, CEDENNA, Universidad de Santiago de Chile, 9170124, Santiago, Chile*

[2]*Universidad Diego Portales, Ejército 441, Santiago, Chile*

[3]*Departamento de Física, Universidade Federal de Viçosa, 36570-900, Viçosa, Brazil*

(Received 29 January 2023; revised 16 June 2023; accepted 30 August 2023; published 27 September 2023)

In this paper, we address the skyrmion-bimeron dynamical transformation during the propagation of such structures along a magnetic nanotrack with anisotropy gradients. Using a micromagnetic approach and simulations, we observe that a skyrmion continuously transforms into a bimeron, and vice versa (in a reversible way). Furthermore, our results show that the topological charge and the velocity of the intermediary magnetic textures emerging during the transformation are constant. These results can contribute to understanding the dynamic transformation between solitonic magnetic textures with the same topological charge.

DOI: 10.1103/PhysRevB.108.094436

During the last decade, the study of magnetic skyrmions has aroused much interest due to their fascinating basic properties and strong potential for applications related to high-density data storage and logic devices [1–6]. This potential emerges from several characteristics that skyrmions exhibit, such as their current-driven transport that requires smaller currents than other spin textures [7–9] and their topology that provides a significant energy barrier to avoid skyrmion annihilation, preventing data loss from thermal fluctuations [1,10,11]. In addition, although skyrmion radii [12] are, in general, greater than vortex core sizes [13–16], the former have a smaller size than other textures, such as skyrmioniums, magnetic bubbles, and others [17–23]. Usually skyrmion-based technological propositions demand the displacement of these topological textures under external stimuli applied along a strip [1,2,24–27]. Therefore, analyzing their dynamical properties under different contexts is a topic of intense research [28–35].

Another two-dimensional (2D) magnetic texture whose properties have been widely studied is the bimeron [36–42], which consists of a meron and an antimeron with opposite polarities and can be viewed as a magnetic skyrmion in a bidimensional magnet. Bimerons also share several appealing properties with skyrmions, making these structures suitable for applications in spintronic devices [42–44] as well. Therefore, authors of several recent studies have focused on the dynamic properties of bimerons under different external stimuli [41,42,45,46], revealing that, as skyrmions, bimerons also present the skyrmion Hall effect [47], a transverse drift during force-driven propagation [46]. However, structural changes in the shape of the bimeron during its displacement allow it to remain in a magnetic nanostripe for longer distances than the skyrmion before annihilating itself at a racetrack border [42].

Topological spin textures can be formally described inside the homotopy theory [48,49]. This formalism describes solitons by mapping the spin-space sphere S onto the physical space. Therefore, skyrmions emerge as solitonic textures belonging to the second homotopy group $\Pi_2(S)$ and are characterized by a topological charge Q, representing the number of times the spin sphere covers the physical space. This mapping can be represented by $\Pi_2(S) = Q$ [48,49]. Under this framework, Belavin-Polyakov skyrmion configurations [50] with $Q = \pm 1$ can have two faces, depending on the boundary conditions (spin stereographic projection). Indeed, the $O(3)$ symmetry allows us to look at the situation as follows: For a skyrmion, we have $\mathbf{m}(r \to \pm\infty) \to (0, 0, \pm 1)$, and for a bimeron, $\mathbf{m}(r \to \pm\infty) \to (0, \pm 1, 0)$, where $r = \sqrt{x^2 + y^2}$, and $\mathbf{m}(\mathbf{r}) \in S$ is the normalized magnetization vector, with $m^2 = 1$. In an isotropic theoretical model, both configurations have the same topological properties. Nevertheless, depending on parameters like small anisotropies, external magnetic fields, or others favoring out-of-plane or in-plane spins, structures like skyrmions or bimerons, respectively, could be excited [51]. Indeed, Ohara *et al.* [52] showed that variations in the external magnetic field and perpendicular magnetic anisotropy nucleate isolated skyrmions and transform them into isolated bimerons in a magnetic disk. Thus, one can conjecture that properly tuning the anisotropy of magnetic nanotracks should allow the dynamical conversion between skyrmions and bimerons during their current-driven motions.

Based on the above, in this paper, we study the dynamical and reversible conversion of current-driven skyrmions into bimerons displacing along a thin ferromagnetic stripe whose anisotropy varies from out-of-plane to in-plane along the nanotrack length. To analyze the dependence on the anisotropy needed for the skyrmion and bimeron stabilization, we start considering the 2D-isotropic ferromagnet described by the nonlinear σ model, given by $\mathcal{H} = \zeta A \int (\nabla \mathbf{m})^2 dS$, where A is the exchange stiffness, ζ is a constant depending on the crystalline structure of the material [53], $\mathbf{m} = \mathbf{M}/M_s$, and M_s is the saturation magnetization. From parametrizing $\mathbf{m} = (\sin\theta\cos\phi, \sin\theta\sin\phi, \cos\theta)$, one can obtain two equivalent

*sebastian.allende@usach.cl

solitonic static solutions having the same exchange energy, depending on the boundary conditions: A skyrmion centered at the origin with radius $R_s = d_s/2$, given by $\phi_s = \arctan(y/x)$ and $\theta_s = \arccos[(d_s^2 - r^2)/d_s^2 + r^2]$, and a bimeron with the merons separated by a distance $R_b = d_b/2$ and its center of mass at the origin. The latter texture can be described as $\phi_b = \arctan[(x - d_b)/y] - \arctan[(x + d_b)/y] - \pi/2$ and $\theta_b = \arccos[R_b x/(r^2 + d_b^2)]$. Nevertheless, the nucleation of different types of solitons in the same material is not usual since each texture results from different energetic equilibria.

Looking for such a possibility, we assume a chiral and anisotropic magnetic system described by

$$E = \int [A\,(\nabla \mathbf{m})^2 + D\,\mathbf{m} \cdot (\nabla \times \mathbf{m}) + K(\mathbf{m} \cdot z)^2]\,dV, \quad (1)$$

where the first, second, and third terms in Eq. (1) are the exchange, Dzyaloshinskii-Moriya (DM), and anisotropy contributions to the magnetic energy, with D and K the DM and anisotropy constants, respectively. One can notice that $K > 0$ ($K < 0$) favors the spin alignment along the in-plane (out-of-plane) direction. Therefore, we can analyze the difference in the energies of the above-described skyrmion and bimeron as a function of K. For all our calculations, we consider that the material parameters are an exchange stiffness $A = 8.78 \times 10^{-12}$ J/m, a saturation magnetization $M_s = 1.1 \times 10^5$ A/m, and a bulk DM constant given by $D = 1.5$ mJ/m^3. These values are in the order of magnitude of the parameters characterizing several magnetic materials such as FeGe [30,54].

We now evaluate Eq. (1) considering both magnetization profiles, the bimeron and the skyrmion. For such calculation, we run micromagnetic simulations to obtain values for R_s and R_b. These simulations will be presented later in this paper, giving $R_s = 27$ nm and $R_b = 9$ nm. Figure 1(c) illustrates both energies for K ranging from -200×10^{-3} to 200×10^{-3} J/m^3. One can notice that the skyrmion is the lower-energy state up to $K \lesssim -45$ J/m^3, while the bimeron becomes the lower-energy configuration for larger values of K. This finding allows us to conjecture the possibility of a reversible dynamical transformation of skyrmions into bimerons when these structures displace along a ferromagnetic nanotrack with varying anisotropy. We highlight that we are dealing with a very thin system in such a way that the magnetostatic contribution can be reduced to an effective easy-surface anisotropy [55–58], which results in a shift of the anisotropy constant $K \to K - \mu_0 M_s^2/2$. This approximation is widely used to describe statics and dynamics of skyrmions [59–61].

To find such behavior, we performed micromagnetic simulations considering a FeGe thin ferromagnetic stripe with length $l = \overline{SB} = 1750$ nm, thickness $h = 10$ nm, and width $w = 1000$ nm, as shown in Fig. 2(a), using a cell size for the simulations of $1 \times 1 \times 1$ nm^3. These geometrical parameters were selected to guarantee enough volume to nucleate stable skyrmions and bimerons. To ensure the stability of skyrmions and bimerons at the ends of the racetrack, we divided it into three regions according to the anisotropy in each. In the region limited by S and O, $\overline{SO} = 250$ nm, as shown in Fig. 2, there is a constant easy-axis anisotropy along the z direction defined by the constant $K_{SO} = 2.5 \times 10^5$ J/m^3. In the region between L and B, $\overline{LB} = 250$ nm, there is an easy-plane anisotropy pointing along the y direction, defined

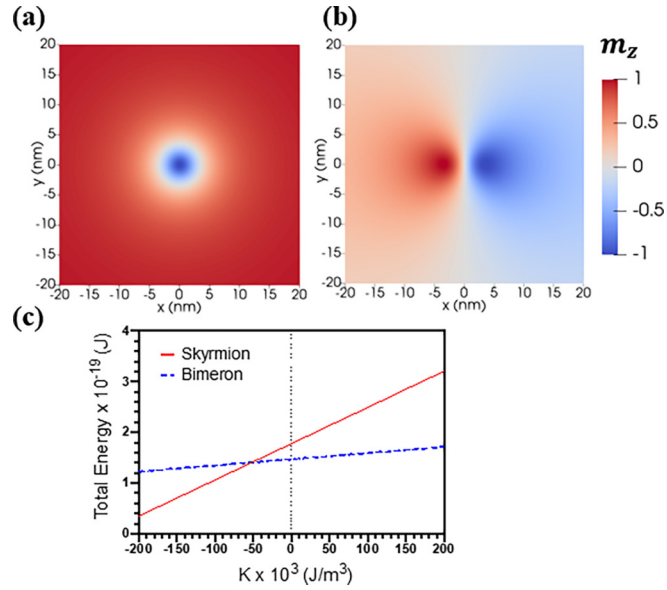

FIG. 1. Magnetization component along the z axis for (a) a skyrmion and (b) a bimeron obtained from the adopted analytical model. (c) The magnetic energy of a skyrmion (red line) and a bimeron (blue-dashed line) is a function of the anisotropy constant. The color bar represents the z component of the magnetization in (a) and (b).

by an anisotropy constant $K_{LB} = 1.4 \times 10^5$ J/m^3. Finally, in the intermediate region $\overline{OL} = 1250$ nm, we consider that the anisotropy axis continuously rotates $\sim 1^0$, while the soliton displaces 15 nm. The easy-axis anisotropy changes from

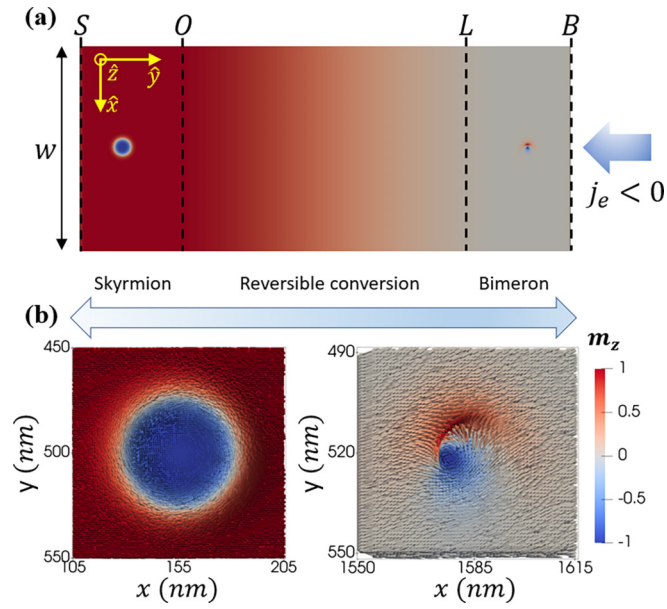

FIG. 2. Panel (a) represents a nanotrack divided into three regions defined by the anisotropy direction. Panel (b) illustrates the skyrmion and bimeron profiles stabilized in the regions $\overline{SO}$ and $\overline{LB}$, respectively. x and y axes in panel (b) show the position coordinates along the nanotrack. The color bar represents the z component of the magnetization in (a) and (b).

out-of-plane to in-plane along the $\overline{OL}$ region. In addition, the anisotropy constant changes linearly from 2.5×10^5 J/m^3 at O in Fig. 2 to 1.4×10^5 J/m^3 at L.

For our simulations, we use the micromagnetic code MUMAX3 [62], a numerical time integration of the Landau-Lifshitz-Gilbert-Slonczewski (LLGS) equation widely used which exhibits good agreement with several experimental results concerning skyrmions. The LLGS equation is defined as

$$\frac{d\mathbf{m}}{dt} = -\gamma_0 \left(\mathbf{m} \times \mathbf{H}_{\text{eff}}\right) + \alpha\left(\mathbf{m} \times \frac{d\mathbf{m}}{dt}\right) + \boldsymbol{\tau}_{\text{stt}}, \qquad (2)$$

where $\gamma_0 = \mu_0\gamma$, γ is the gyromagnetic ratio, μ_0 is the magnetic permeability, and α is the Gilbert damping constant. Here, $\mathbf{H}_{\text{eff}}$ is the effective field given by the sum of the exchange, dipolar, anisotropy, and bulk DM energy contributions. All the simulations include these four energy contributions. Additionally, $\boldsymbol{\tau}_{\text{stt}}$ is the spin transfer torque term, given by

$$\boldsymbol{\tau}_{\text{stt}} = -(\mathbf{v}_j \cdot \nabla)\mathbf{m} + \beta\mathbf{m} \times (\mathbf{v}_j \cdot \nabla)\mathbf{m}, \qquad (3)$$

where $\mathbf{v}_j = -\mu_B P \mathbf{j}_e/[eM_s(1+\beta^2)]$, $\mathbf{j}_e$ is the spin-polarized current density, $P = 0.5$ is the polarization rate of the current, e is the electronic charge, and β gives the degree of nonadiabaticity. To study only the skyrmion-bimeron conversion, we consider the parameters $\alpha = \beta = 0.1$ to avoid the skyrmion Hall effect [4,63,64]. To visualize the magnetization obtained in MUMAX3, we use Paraview [65].

We start our simulation by nucleating a skyrmion at the $\overline{SO}$ region. After that, we apply a spin-polarized current density pointing from right to left ($-y$ direction) along the larger side of the stripe $j_e = -4 \times 10^{12}$ A/m^2. This current density allows the skyrmion to propagate along the stripe, going to the $\overline{OL}$ region. Figure 3 shows the evolution of the solitonic texture while propagating along the region $\overline{OL}$. At $t = 0$, a perfect skyrmion is presented with m_z showing a circular symmetry in the xy plane, as seen in Fig. 3. After $t \approx 0.34$ ns, the skyrmion loses its circular symmetry, forming an ellipticallike magnetic texture. Nevertheless, m_y starts acquiring a circular symmetry along the xy plane, as shown in Fig. 3(b). Finally, at $t \approx 1.24$ ns, when the soliton reaches the $\overline{LB}$ region, it completely transforms into a bimeron.

Once the bimeron is at the right extreme of the racetrack, we change the direction of the current density, and the bimeron starts propagating through the $\overline{SO}$ region, where a skyrmion appears. Therefore, the described phenomenon is reversible. A video showing the skyrmion-bimeron transformation is included as Supplemental Material [66].

To clarify the transformation process, we obtain the topological charge $Q = (4\pi)^{-1} \int dS\, \mathbf{m} \cdot (\partial_x\mathbf{m} \times \partial_y\mathbf{m})$ of the magnetic texture during the dynamics. Our results are illustrated in Fig. 4(a), showing that Q is constant during all the motion of the soliton and close to -1. Small deviations from the unity of the topological charge appear due to the finite size of the soliton that creates small numerical artifacts. This behavior indicates that the soliton keeps its topological protection against configurations belonging to other topological sectors with different values of Q.

Furthermore, the analysis of the soliton position as a function of time presented in Fig. 4(b) evidences that the magnetic

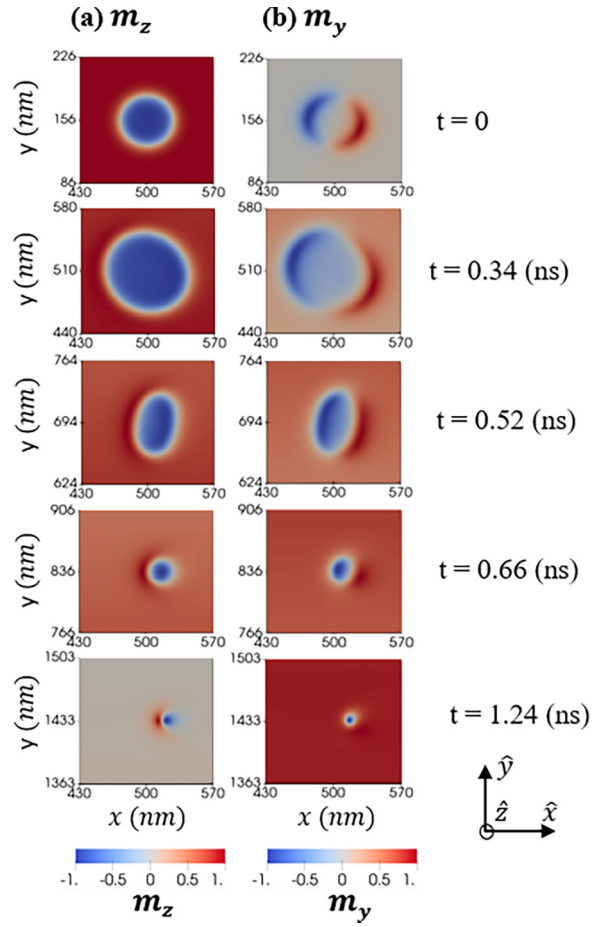

FIG. 3. Magnetization components as a function of time of the conversion of the skyrmion into a bimeron. Panels (a) and (b) illustrate the magnetization along the z and y directions, respectively. x and y axes show the coordinates of the position along the nanotrack, according to the coordinate system shown in the inset. The color bar represents the z component of the magnetization in (a) and the y component of the magnetization in (b).

texture has a constant velocity during its propagation along the nanostripe while changing from skyrmion into bimeron and vice versa.

To understand the constant velocity of the soliton texture, we qualitatively analyze its dynamics from the perspective of the generalized Thiele equation [67,68]: $\mathcal{G}\mathbf{z} \times (\mathbf{v}_j - \mathbf{v}_s) + \overleftrightarrow{\mathcal{D}}(\beta\mathbf{v}_j - \alpha\mathbf{v}_s) = \mathbf{F}$, where $\mathcal{G}\mathbf{z} = M_s\gamma^{-1}\int \mathbf{m} \cdot (\partial_x\mathbf{m} \times \partial_y\mathbf{m})\, dV$ is the gyrovector, $\overleftrightarrow{\mathcal{D}}$ is the dissipative dyadic tensor, whose elements are $\mathcal{D}_{ij} = M_s\gamma^{-1}\int(\partial_i\mathbf{m} \cdot \partial_i\mathbf{m})\, dV$, and $\mathbf{v}_s$ is the soliton drift velocity. Although the Thiele equation should be used to describe the dynamics of magnetic textures considered rigid bodies, the results obtained from our simulations allow us to use this approach to analyze the soliton motion. Indeed, from considering the initial (skyrmion) and final (bimeron) textures, the effects of variations in their gyrovector and diagonal elements of the dyadic tensor produce very small variations in the soliton velocity (see details in Supplemental Material [66]). Therefore, although the intermediary configurations do not share the symmetries of the skyrmion and bimeron, the Thiele equation accounts for the main aspects

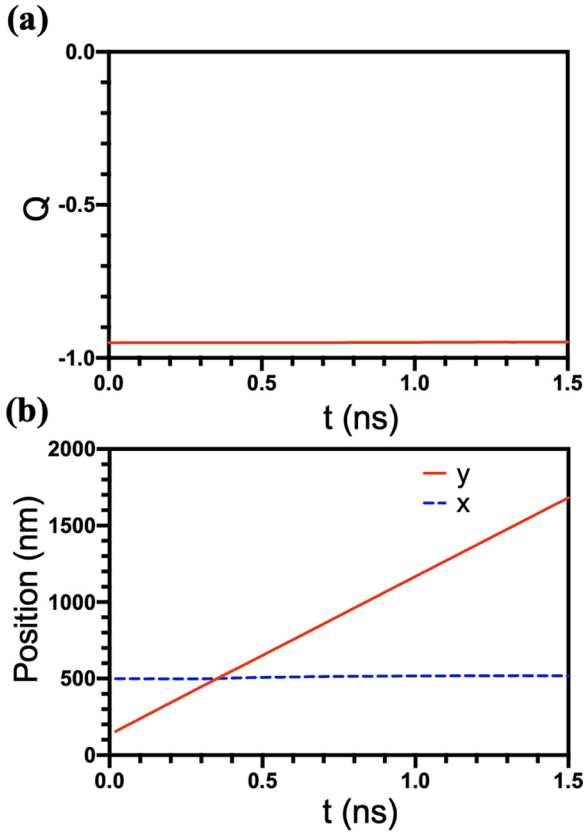

FIG. 4. Panel (a) presents the topological charge of the soliton as a function of the time. Panel (b) shows the magnetic texture position along y (red line) and x (blue-dashed line) directions as a function of time.

of soliton dynamics. Under these assumptions, we obtain that the soliton velocity along the racetrack is given by

$$\mathbf{v}_s = -\frac{\mu_B P}{eM_s(1+\beta^2)}\,\mathbf{j}_e, \tag{4}$$

independent of the shape of the magnetic solitonic texture. We call attention to the fact that we are considering $\alpha = \beta$ so that the skyrmion velocity perpendicular to the propagation direction vanishes [68]. This transformation from skyrmion to bimeron with a conserved topological charge is also observed when the skyrmion Hall effect is present, i.e., when considering $\alpha = 0.1$ and $\beta = 0.05$. The only difference when comparing results in the latter case with those reported in Fig. 4(b) is a change in the magnetic texture position in the x axis as a function of time due to the skyrmion Hall effect. That is, since $\mathbf{v}_x$ strongly depends on β, if we increase β, the Hall effect will rapidly annihilate the soliton. However, $\mathbf{v}_y$ exhibits a smaller β dependence, and no relevant changes in the soliton propagation along this direction appear. Detailed results and equations illustrating this dependence are included as Supplemental Material [66]. We also highlight that our simulations reveal that the anisotropy gradient is responsible for a skyrmion motion even for a null electric current. The associated velocities are two orders of magnitude smaller than those obtained when we apply an electric current. It is not possible to stabilize the skyrmion position inside the

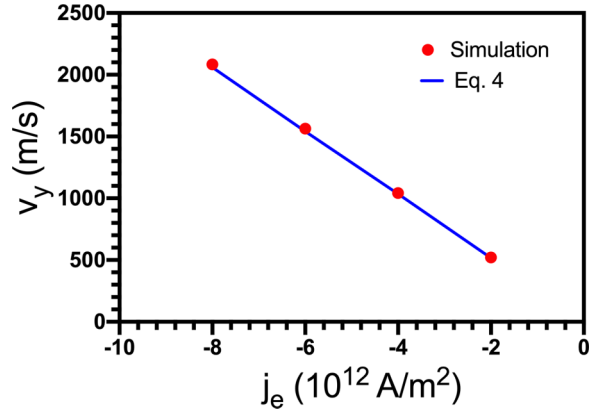

FIG. 5. Velocity of the soliton along the y direction as a function of the spin-polarized current density. Dots represent the data obtained from simulations, and the blue line corresponds to Eq. (4).

transition zone since any fluctuation will produce the propagation of the soliton. To stabilize it, additional mechanisms such as notches are required. To overcome the anisotropy gradient drift, a minimum current density is needed. However, the analysis of this phenomenon is out of the scope of this paper.

Finally, to corroborate the above statements, we analyze the soliton velocity as a function of the current density obtained from our micromagnetic simulations (red dots) and the Thiele analytical approach presented in Eq. (4) (blue line). Results are presented in Fig. 5, evidencing an excellent agreement between both approaches and a linear dependence of the soliton velocity on the spin-polarized current density in the range of -8×10^{12} to -2×10^{12} A/m^2. The phenomenology of the skyrmion-bimeron transformation is also observed when an interfacial DM interaction is considered, as shown in Fig. S3 of the Supplemental Material [66]. However, since the interfacial DM interaction yields a Néel skyrmion [1,44], the bimeron profile obtained with such a DM interaction is different from the bimeron originated from bulk DM interaction. Therefore, Bloch and Néel skyrmions are, respectively, transformed in the here-called Bloch and Néel bimerons, whose profiles are depicted in Fig. 6.

In conclusion, we have studied the dynamics of a skyrmion through a ferromagnetic stripe whose anisotropy rotates

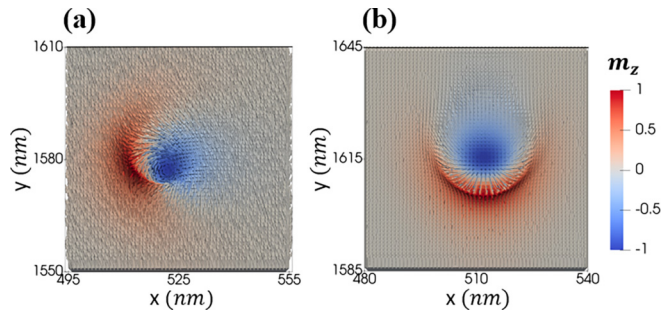

FIG. 6. Magnetization patterns of (a) a Bloch and (b) a Néel bimeron. x and y axes show the position components along the nanotrack.

continuously from out-of-plane to in-plane. Such a rotation yields the soliton deforms while propagating along the nanostripe, continuously transforming into a bimeron. During the transformation, the topological charge and the velocity of the magnetic texture are constant. We also observe that the transformation from skyrmion to bimeron is reversible. These results could be used to design spintronic devices demanding the presence of different solitonic spin textures in the same system.

We acknowledge financial support in Chile from FONDECYT Grants No. 1200867 and No. 1220215, and Financiamiento Basal para Centros Científicos y Tecnológicos de Excelencia AFB220001. M.C. acknowledges Proyecto Postdoc DICYT, Código 042231AP_POSTDOC, Vicerrectoría de Investigación, Desarrollo e Innovación. D.G.-P. acknowledges ANID-Subdirección de Capital Humano/Doctorado Nacional/2023-21230818. In Brazil, we thank the INCT of Spintronics and Advanced Magnetic Nanostructures (INCT-SpinNanoMag), and the agencies CNPq (Grants No. 305256/2022-0) and Fapemig (Grant No. APQ-00648-22). V.L.C.-S. thanks Cedenna and Universidad de Santiago de Chile for hospitality. We thank G. Romero for the fruitful discussions.

[1] A. Fert, V. Cros, and J. Sampaio, Skyrmions on the track, Nat. Nanotechnol. **8**, 152 (2013).
[2] X. Zhang, Y. Zhou, M. Ezawa, G. P. Zhao, and W. Zhao, Magnetic skyrmion transistor: Skyrmion motion in a voltage-gated nanotrack, Sci. Rep. **5**, 11369 (2015).
[3] J. Iwasaki, M. Mochizuki, and N. Nagaosa, Current-induced skyrmion dynamics in constricted geometries, Nat. Nanotechnol. **8**, 742 (2013).
[4] J. Sampaio, V. Cros, S. Rohart, A. Thiaville, and A. Fert, Nucleation, stability and current-induced motion of isolated magnetic skyrmions in nanostructures, Nat. Nanotechnol. **8**, 839 (2013).
[5] X. Zhang, M. Ezawa, and Y. Zhou, Magnetic skyrmion logic gates: Conversion, duplication and merging of skyrmions, Sci. Rep. **5**, 9400 (2015).
[6] X. Zhang, G. P. Zhao, H. Fangohr, J. P. Liu, W. X. Xia, J. Xia, and F. J. Morvan, Skyrmion-skyrmion and skyrmion-edge repulsions in skyrmion-based racetrack memory, Sci. Rep. **5**, 7643 (2015).
[7] F. Jonietz, S. Mühlbauer, C. Pfleiderer, A. Neubauer, W. Münzer, A. Bauer, T. Adams, R. Georgii, P. Böni, R. A. Duine, K. Everschor, M. Garst, and A. Rosch, Spin transfer torques in MnSi at ultralow current densities, Science **330**, 1648 (2010).
[8] N. Romming, C. Hanneken, M. Menzel, J. E. Bickel, B. Wolter, K. von Bergmann, A. Kubetzka, and R. Wiesendanger, Writing and deleting single magnetic skyrmions, Science **341**, 636 (2013).
[9] X. Z. Yu, N. Kanazawa, W. Z. Zhang, T. Nagai, T. Hara, K. Kimoto, Y. Matsui, Y. Onose, and Y. Tokura, Skyrmion flow near room temperature in an ultralow current density, Nat. Commun. **3**, 988 (2012).
[10] P. F. Bessarab, V. M. Uzdin, and H. Jónsson, Method for finding mechanism and activation energy of magnetic transitions, applied to skyrmion and antivortex annihilation, Comput. Phys. Commun. **196**, 335 (2015).
[11] D. Cortés-Ortuño, W. Wang, M. Beg, R. A. Pepper, M.-A. Bisotti, R. Carey, M. Vousden, T. Kluyver, O. Hovorka, and H. Fangohr, Thermal stability and topological protection of skyrmions in nanotracks, Sci. Rep. **7**, 4060 (2017).
[12] H. Wu, X. Hu, K. Jing, and X. R. Wang, Size and profile of skyrmions in skyrmion crystals, Commun. Phys. **4**, 210 (2021).
[13] X. S. Wang, H. Y. Yuan, and X. R. Wang, A theory on skyrmion size, Commun. Phys. **1**, 31 (2018).
[14] G. Finocchio, F. Büttner, R. Tomasello, M. Carpentieri, and M. Kläui, Magnetic skyrmions: From fundamental to applications, J. Phys. D **49**, 423001 (2016).
[15] C. Holl, M. Knol, M. Pratzer, J. Chico, I. L. Fernandes, S. Lounis, and M. Morgenstern, Probing the pinning strength of magnetic vortex cores with sub-nanometer resolution, Nat. Commun. **11**, 2833 (2020).
[16] E. R. P. Novais, P. Landeros, A. G. S. Barbosa, M. D. Martins, F. Garcia, and A. P. Guimarães, Properties of magnetic nanodots with perpendicular anisotropy, J. Appl. Phys. **110**, 053917 (2011).
[17] S. Parkin and S.-H. Yang, Memory on the racetrack, Nat. Nanotechnol. **10**, 195 (2015).
[18] A. Thiaville and Y. Nakatani, Domain-wall dynamics in nanowires and nanostrips, in *Topics in Applied Physics: Spin Dynamics in Confined Magnetic Structures III*, edited by B. Hillebrands and A. Thiavile (Springer-Verlag, Heidelberg, 2006).
[19] S. Jamet, N. Rougemaille, J.-C. Toussaint, and O. Fruchart, 25 - *Head-to-Head Domain Walls in One-Dimensional Nanostructures: An Extended Phase Diagram Ranging from Strips to Cylindrical Wires*, edited by Manuel Vázquez, Woodhead Publishing Series in Electronic and Optical Materials, Magnetic Nano- and Microwires (Woodhead Publishing, 2015).
[20] B. Göbel, A. F. Schäffer, J. Berakdar, I. Mertig, and S. S. P. Parkin, Electrical writing, deleting, reading, and moving of magnetic skyrmioniums in a racetrack device, Sci. Rep. **9**, 12119 (2019).
[21] J. Xia, X. Zhang, X. Liu, Y. Zhou, and M. Ezawa, Qubits based on merons in magnetic nanodisks, Commun. Mater. **3**, 88 (2022).
[22] B. Göbel, I. Mertig, and O. A. Tretiakov, Beyond skyrmions: Review and perspectives of alternative magnetic quasiparticles, Phys. Rep. **895**, 1 (2021).
[23] A. P. Malozemoff and J. C. Slonczewski, *Magnetic Domain Walls in Bubble Materials* (Academic Press, New York, United States, 1979).
[24] P. Upadhyaya, G. Yu, P. K. Amiri, and K. L. Wang, Electric-field guiding of magnetic skyrmions, Phys. Rev. B **92**, 134411 (2015).
[25] S. Woo, K. Litzius, B. Krüger, M.-Y. Im, L. Caretta, K. Richter, M. Mann, A. Krone, R. M. Reeve, M. Weigand, P. Agrawal, I. Lemesh, M.-A. Mawass, P. Fischer, M. Kläui, and G. S. D. Beach, Observation of room-temperature magnetic skyrmions and their current-driven dynamics in ultrathin metallic ferromagnets, Nat. Mater. **15**, 501 (2016).
[26] Y. Zhang, S. Luo, B. Yan, J. Ou-Yang, X. Yang, S. Chen, B. Zhu, and L. You, Magnetic skyrmions without the skyrmion Hall

effect in a magnetic nanotrack with perpendicular anisotropy, Nanoscale **9**, 10212 (2017).
[27] J. C. Martinez, W. S. Lew, W. L. Gan, and M. B. A. Jalil, Theory of current-induced skyrmion dynamics close to a boundary, J. Magn. Magn. Mater. **465**, 685 (2018).
[28] K. V. Yershov, A. Kákay, and V. P. Kravchuk, Curvature-induced drift and deformation of magnetic skyrmions: Comparison of the ferromagnetic and antiferromagnetic cases, Phys. Rev. B **105**, 054425 (2022).
[29] V. L. Carvalho-Santos, M. A. Castro, D. Salazar-Aravena, D. Laroze, R. M. Corona, S. Allende, and D. Altbir, Skyrmion propagation along curved racetracks, Appl. Phys. Lett. **118**, 172407 (2021).
[30] X. Wang, X. S. Wang, C. Wang, H. Yang, Y. Cao, and P. Yan, Current-induced skyrmion motion on magnetic nanotubes, J. Phys. D: Appl. Phys. **52**, 225001 (2019).
[31] C. Reichhardt, C. J. O. Reichhardt, and M. V. Milošević, Statics and dynamics of skyrmions interacting with disorder and nanostructures, Rev. Mod. Phys. **94**, 035005 (2022).
[32] K. Everschor-Sitte, J. Masell, R. M. Reeve, and M. Kläui, Perspective: Magnetic skyrmions—Overview of recent progress in an active research field, J. Appl. Phys. **124**, 240901 (2018).
[33] Z. Chen, X. Zhang, Y. Zhou, and Q. Shao, Skyrmion Dynamics in the Presence of Deformation, Phys. Rev. Appl. **17**, L011002 (2022).
[34] R. C. Silva, R. L. Silva, V. L. Carvalho-Santos, W. A. Moura-Melo, and A. R. Pereira, Skyrmion bound state and dynamics in an antiferromagnetic bilayer racetrack, J. Magn. Magn. Mater. **549**, 168997 (2022).
[35] S. Vojkovic, R. Cacilhas, A. R. Pereira, D. Altbir, Á. S. Núñez, and V. L. Carvalho-Santos, Scattering modes of skyrmions in a bilayer system with ferromagnetic coupling, Nanotechnology **32**, 175702 (2021).
[36] M. A. Amaral, R. L. Silva, A. R. Pereira, and W. A. Moura-Melo, Discrete double core skyrmions in magnetic thin films, J. Magn. Magn. Mater. **321**, 3360 (2009).
[37] R. L. Fernandes, R. J. C. Lopes, and A. R. Pereira, Skyrmions and merons in two-dimensional antiferromagnetic systems, Solid State Commun. **290**, 55 (2019).
[38] B. Göbel, A. Mook, J. Henk, I. Mertig, and O. A. Tretiakov, Magnetic bimerons as skyrmion analogues in in-plane magnets, Phys. Rev. B **99**, 060407(R) (2019).
[39] R. L. Silva, L. D. Secchin, W. A. Moura-Melo, A. R. Pereira, and R. L. Stamps, Emergence of skyrmion lattices and bimerons in chiral magnetic thin films with nonmagnetic impurities, Phys. Rev. B **89**, 054434 (2014).
[40] I. A. Iakovlev, O. M. Sotnikov, and V. V. Mazurenko, Bimeron nanoconfined design, Phys. Rev. B **97**, 184415 (2018).
[41] X. Zhang, J. Xia, L. Shen, M. Ezawa, O. A. Tretiakov, G. Zhao, X. Liu, and Y. Zhou, Static and dynamic properties of bimerons in a frustrated ferromagnetic monolayer, Phys. Rev. B **101**, 144435 (2020).
[42] A. S. Araújo, R. J. C. Lopes, V. L. Carvalho-Santos, A. R. Pereira, R. L. Silva, R. C. Silva, and D. Altbir, Typical skyrmions versus bimerons: A long-distance competition in ferromagnetic racetracks, Phys. Rev. B **102**, 104409 (2020).
[43] R. Tomasello, E. Martinez, R. Zivieri, L. Torres, M. Carpentieri, and G. Finocchio, A strategy for the design of skyrmion racetrack memories, Sci. Rep. **4**, 6784 (2014).
[44] S. Luo and L. You, Skyrmion devices for memory and logic applications, APL Mater. **9**, 050901 (2021).
[45] L. Shen, J. Xia, X. Zhang, M. Ezawa, O. A. Tretiakov, X. Liu, G. Zhao, and Y. Zhou, Current-Induced Dynamics and Chaos of Antiferromagnetic Bimerons, Phys. Rev. Lett. **124**, 037202 (2020).
[46] L. Shen, X. Li, J. Xia, L. Qiu, X. Zhang, O. A. Tretiakov, M. Ezawa, and Y. Zhou, Dynamics of ferromagnetic bimerons driven by spin currents and magnetic fields, Phys. Rev. B **102**, 104427 (2020).
[47] K. Litzius, I. Lemesh, B. Krüger, P. Bassirian, L. Caretta, K. Richter, F. Büttner, K. Sato, O. A. Tretiakov, J. Förster, R. M. Reeve, M. Weigand, I. Bykova, H. Stoll, G. Schütz, G. S. D. Beach, and M. Kläui, Skyrmion Hall effect revealed by direct time-resolved x-ray microscopy, Nat. Phys. **13**, 170 (2017).
[48] N. D. Mermin, The topological theory of defects in ordered media, Rev. Mod. Phys. **51**, 591 (1979).
[49] R. Rajaraman, *Solitons and Instantons: An introduction to Solitons and Instantons in Quantum Field Theory* (North Holland, Amsterdam, 1982).
[50] A. A. Belavin and A. M. Polyakov, Metastable states of two-dimensional isotropic ferromagnets, JETP Lett. **22**, 245 (1975).
[51] Y. A. Kharkov, O. P. Sushkov, and M. Mostovoy, Bound States of Skyrmions and Merons near the Lifshitz Point, Phys. Rev. Lett. **119**, 207201 (2017).
[52] K. Ohara, X. Zhang, Y. Chen, S. Kato, J. Xia, M. Ezawa, O. A. Tretiakov, Z. Hou, Y. Zhou, G. Zhao, J. Yang, and X. Liu, Reversible Transformation between isolated skyrmions and bimerons, Nano Lett. **22**, 8559 (2022).
[53] A. Aharoni, *Introduction to the Theory of Ferromagnetism* (Oxford University Press, New York, 1996).
[54] K. Niitsu, Y. Liu, A. C. Booth, X. Yu, N. Mathur, M. J. Stolt, D. Shindo, S. Jin, J. Zang, N. Nagaosa, and Y. Tokura, Geometrically stabilized skyrmionic vortex in FeGe tetrahedral nanoparticles, Nat. Mater. **21**, 305 (2022).
[55] V. Slastikov, Micromagnetism of thin shell, Math. Models Methods Appl. Sci. **15**, 1469 (2005).
[56] G. Gioia and R. D. James, Micromagnetics of very thin films, Proc. R. Soc. London A **453**, 213 (1997).
[57] R. V. Kohn and V. V. Slastikov, Effective dynamics for ferromagnetic thin films: A rigorous justification, Proc. R. Soc. London A **461**, 143 (2005).
[58] K. V. Yershov, V. P. Kravchuk, D. D. Sheka, and U. K. Rößler, Curvature effects on phase transitions in chiral magnets, SciPost Phys. **9**, 043 (2020).
[59] V. P. Kravchuk, U. K. Rößler, O. M. Volkov, D. D. Sheka, J. van den Brink, D. Makarov, H. Fuchs, H. Fangohr and Y. Gaididei, Topologically stable magnetization states on a spherical shell: Curvature-stabilized skyrmions, Phys. Rev. B **94**, 144402 (2016).
[60] V. P. Kravchuk, D. D. Sheka, A. Kákay, O. M. Volkov, U. K. Rößler, J. van den Brink, D. Makarov, and Y. Gaididei, Multiplet of Skyrmion States on a Curvilinear Defect: Reconfigurable Skyrmion Lattices, Phys. Rev. Lett. **120**, 067201 (2018).
[61] O. V. Pylypovskyi, D. Makarov, V. P. Kravchuk, Y. Gaididei, A. Saxena, and D. D. Sheka, Chiral Skyrmion and Skyrmionium

States Engineered by the Gradient of Curvature, Phys. Rev. Appl. **10**, 064057 (2018).

[62] A. Vansteenkiste, J. Leliaert, M. Dvornik, M. Helsen, F. Garcia-Sanchez, and B. Van Waeyenberge, The design and verification of MuMax3, AIP Adv. **4**, 107133 (2014).

[63] W. Koshibae and N. Nagaosa, Theory of current-driven skyrmions in disordered magnets, Sci. Rep. **8**, 6328 (2018).

[64] C. Deger, I. Yavuz, and F. Yildiz, Current-driven coherent skyrmion generation, Sci. Rep. **9**, 3513 (2019).

[65] J. Ahrens, B. Geveci, and C. Law, *ParaView: An End-User Tool for Large-Data Visualization*, Visualization Handbook (Elsevier, 2005), pp. 717–731.

[66] See Supplemental Material at http://link.aps.org/supplemental/10.1103/PhysRevB.108.094436 for details on the dependence on β of the skyrmion-bimeron transformation. It also contains the phenomenology of the skyrmion-bimeron transformation for an interfacial DM interaction and the details on the calculation of the soliton velocity. Finally, It contains a video presenting the transformation from the skyrmion into a bimeron.

[67] A. A. Thiele, Steady-State Motion of Magnetic Domains, Phys. Rev. Lett. **30**, 230 (1973).

[68] J. C. Martinez and M. B. A. Jalil, Topological dynamics and current-induced motion in a skyrmion lattice, New J. Phys. **18**, 033008 (2016).